POLITECNICO
MILANO 1863

SCUOLA DI INGEGNERIA INDUSTRIALE
E DELL'INFORMAZIONE

Executive Summary of the Thesis

Monolithic and hybrid semiconductor photonic devices for quantum information

Laurea Magistrale in Engineering Physics - Ingegneria Fisica

Author: Lorenzo Lazzari

Advisor: Prof. Roberto Osellame

Co-advisor: Sara Ducci

Academic year: 2021-2022

1. Introduction

Following the emergence of quantum information (QI) over the last three decades, the demand of physical systems supporting or generating controllable quantum states has drastically increased. In fact, the quantum properties of such states – from state superposition and non-cloning theorem to entanglement – are exploited to overcome the limits of classical information protocols, pursuing, for example, the establishment of unconditionally secure communications, the creation of new computational tools to address classically unsolvable or inefficient algorithms, the proficient simulation of complex systems. Among all the currently available physical platforms for the development of quantum technologies, spanning from atomic and solid state systems to superconductive circuits, we focus our attention on photons. Thanks to their high speed and immunity to decoherence, they are particularly suited for carrying QI and are employed not only in quantum communication protocols but also in quantum simulation and computing [1].

Qubits, two-level systems representing the basic unit of QI, can be implemented in a large variety of degrees of freedom of photons, including polarization, arrival time at a detector, spatial path, frequency and orbital angular momentum. For this reason, the development of sources of single or entangled photons, such as quantum dots [2] or parametric sources [3], has been a major objective of the last decades. Several material platforms are investigated for the implementation of integrated, robust, controllable, low-power consumption and high fabrication yield devices able to efficiently generate, manipulate, distribute and detect the target quantum states [4, 5]. Light can be, indeed, confined at the micrometer scale via nano-fabricated waveguides, while nonlinear effects can be exploited for the production of photonic qubits.

Here we present the implementation of integrated photonic devices using AlGaAs, a semiconductor III-V material with direct bandgap: we describe the design of a parametric source of entangled photon pairs at room temperature and its characterization in terms of nonlinear performances and entanglement quality. Furthermore, we propose a hybrid device resulting from the heterogeneous integration of the AlGaAs source with a silicon-on-insulator (SOI) circuit, in the aim of merging the two material platforms and leveraging their complementary assets.

2. AlGaAs waveguides as photon-pair sources

AlGaAs Bragg reflection waveguides are designed for efficient nonlinear conversion, making use of modal phase-matching for generating broadband energy-time and polarization entangled bi-photon states.

2.1. Nonlinear optics in waveguides

When intense electromagnetic fields interact with matter, we observe optical phenomena that can only be described with nonlinear equations. Second order nonlinearity is responsible of a series of possible interactions between three fields (*three-wave mixing* processes): in a quantized picture, three photons, each one in a given frequency mode (ω_1, ω_2 or ω_3, such that $\omega_3 = \omega_1 + \omega_2$ for energy conservation), will interact within the nonlinear medium, whose nonlinear properties are described by the susceptibility tensor $\chi^{(2)}$, leading to the creation or annihilation of one of them. If the pump fields are at frequencies ω_1, ω_2 and the generated one is at ω_3, we talk about sum frequency generation (SFG) process.
The amount of generated optical power is proportional to the pump one and to the square of the interacting length; a particular conversion process occurs when the corresponding nonlinear tensor element is non-null and it is efficient only if the phase-matching (PM) condition is satisfied, meaning that the momentum is conserved in the interaction: $\mathbf{k}_3 - \mathbf{k}_1 - \mathbf{k}_2 = 0$, where $\mathbf{k}_i$ is the wavevector of the field i. If the fields are confined in waveguides – in this case, we call them *modes* –, we consider the interplay between the spatial distributions of the interacting fields and $\chi^{(2)}$ by means of the nonlinear overlap integral:

$$\Gamma = \frac{1}{2} \iint_S \mathrm{d}x\mathrm{d}z \chi^{(2)} A_1^* A_2^* A_3, \qquad (1)$$

where S is the transverse section of the waveguide, the reference frame is the one of Figure 1, $A_i(x, z)$ is the normalized transverse spatial distribution ($\iint_S \mathrm{d}x\mathrm{d}z |A_i|^2 = 1$) of mode i at frequency ω_i, propagating along the y direction. The conversion efficiency is, in this case, also proportional to $|\Gamma|^2$: thus, the waveguides are designed in order to maximize the overlap integral and to satisfy the PM condition.

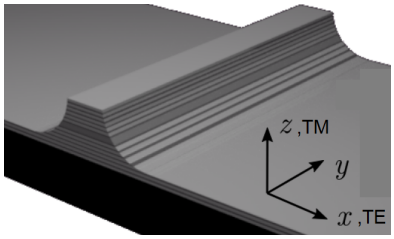

Figure 1: Sketch of the AlGaAs waveguide with reference frame.

2.2. Design

Wavevectors are colinear for waveguide modes. Hence, the PM condition turns into: $n_3\omega_3 = n_1\omega_1 + n_2\omega_2$, being $n_i = n_i(\omega_i)$ the effective refractive index experienced by the mode i at frequency ω_i. For a given mode, this condition is never met, being $n(\omega)$ a monotonic increasing function in the spectral region of interest; for instance, if we consider a so-called second harmonic generation (SHG) process (the degenerate case of SFG: $\omega_1 = \omega_2 = \omega$ and $\omega_3 = 2\omega$), we obtain $n(2\omega) = n(\omega)$, which is clearly in contrast with the function profile. Among the available strategies to overcome this issue, the modal PM method consists of having two modes with different chromatic dispersion (mode u and mode v) supported by the waveguide and involved in the interaction, such that $n_u(2\omega) = n_v(\omega)$.
Horizontally (or TE) and vertically (or TM) polarized fundamental modes in the telecom range are confined in the core of our waveguides by total internal reflection. Bragg reflectors made up of AlGaAs layers in the vertical direction with different Al concentration – thus, different refractive index – confine the so-called TE and TM Bragg modes in the near-infrared (NIR) range [6]. Modal PM can be fulfilled between these interacting modes [7] and the resulting waveguide is sketched in Figure 1.
Besides being suitable to achieve modal PM, AlGaAs is characterized by one of the largest second order nonlinearities [5]. The crystallographic symmetries, which shape the $\chi^{(2)}$, allow three PM conversion processes:

1. **Type 0**: $\omega_B n_{TMB}(\omega_B) = \omega_s n_{TM}(\omega_s) + \omega_i n_{TM}(\omega_i)$;
2. **Type I**: $\omega_B n_{TMB}(\omega_B) = \omega_s n_{TE}(\omega_s) + \omega_i n_{TE}(\omega_i)$;
3. **Type II**: $\omega_B n_{TEB}(\omega_B) = \omega_s n_{TE}(\omega_s) + \omega_i n_{TM}(\omega_i)$,

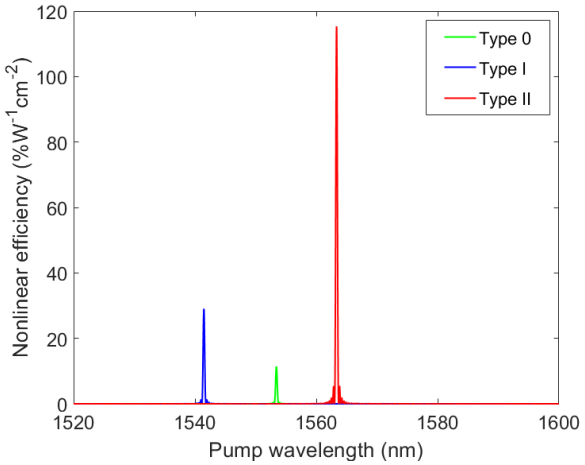

Figure 2: Simulated SHG efficiency curves for the PM types.

where ω_B is the frequency of the Bragg mode, ω_s and ω_i the frequencies of the fundamental modes (such that $\omega_B = \omega_s + \omega_i$), $n_{TE(B)/TM(B)}$ the effective refractive index of the fundamental(Bragg) TE/TM modes. In Figure 2, we display the simulated SHG conversion efficiencies in our structures per unit pump optical power and unit squared interaction length per each PM type; this let us retrieve the PM resonance frequencies, the frequencies of the SHG signals (double the corresponding pump frequencies).

2.3. Generating quantum states

Photon pairs are generated in our waveguides via spontaneous parametric down-conversion (SPDC), which is conceptually the inverse process to SFG: a pump photon at frequency ω_B, triggered by vacuum fluctuations, is down-converted into two photons at frequencies ω_s and ω_i, with $\omega_B = \omega_s + \omega_i$. The produced bi-photon state $|\psi\rangle$ can be written as:

$$|\psi\rangle = \iint \mathrm{d}\omega_s \mathrm{d}\omega_i C(\omega_s, \omega_i) \hat{a}_s^\dagger(\omega_s) \hat{a}_i^\dagger(\omega_i) |0\rangle, \quad (2)$$

where $\hat{a}_x^\dagger(\omega_x)$ is the operator which creates a photon in the mode x with frequency ω_x and $|0\rangle$ is the vacuum state. $C(\omega_s, \omega_i)$ is the joint spectral amplitude (JSA) function, whose modulus squared gives the probability that the bi-photon state is composed by a *signal* photon at frequency ω_s and an *idler* photon at frequency ω_i. It can be re-written as:

$$C(\omega_s, \omega_i) \propto \tilde{\Gamma} \phi_p(\omega_s + \omega_i) \phi_{PM}(\omega_s, \omega_i), \quad (3)$$

where $\tilde{\Gamma}$ is the non-normalized nonlinear overlap (Equation 1), ϕ_p the pump spectral distribution, ϕ_{PM} the phase-matching function. The narrower the spectral width of ϕ_p, the more frequency anti-correlated are the two generated photons; assuming a Dirac delta-like ϕ_p, the bandwidth of the produced bi-photon state will be given by ϕ_{PM}, which accounts for the satisfaction of the PM condition for each considered triplet of interacting photons. The best conversion efficiency is reached when ω_B corresponds to the PM resonance frequency.
A sufficiently narrowband pump makes the photons generated through SPDC to be naturally energy-time and frequency-bin entangled. Furthermore, photons produced via a type 2 PM conversion process are also polarization entangled. All these degrees of freedom can be retrieved and exploited in our structures.

3. Performances characterization

The fabricated waveguides are characterized in terms of optical losses, SHG conversion efficiency, photon-pair production rate and energy-time entanglement visibility, in view of their application to QI protocols and their integration with SOI platforms.

3.1. Nonlinear conversion efficiency

The experimental optical pumping is achieved by using two frequency-tunable narrowband continuous wave (CW) lasers (*Tunics* for the telecom range, *TOPTICA* for the NIR); light is conveyed to the waveguides by means of microscope objectives. The large index mismatch between AlGaAs and air makes the waveguide to behave like an optical cavity, whose facets' reflectivity can be numerically estimated for any given supported mode: the contrast of the resulting Fabry-Perot interference pattern can be used to directly retrieve the optical losses coefficients [8], thus characterizing the transmission of the guide.
A SHG measurement is used to characterize the nonlinear properties of the waveguide, in order to retrieve the PM resonance frequency and the conversion efficiency. The telecom CW laser is used as optical pump: by controlling its polarization, we have access to the different types of PM conversion processes. The produced signal

is detected by a photodiode sensitive to NIR light combined with a signal recovery stage. By estimating the waveguide internal optical power and the coupling efficiency, we calculate the nonlinear conversion efficiency and compare it to the one obtained with simulations (Figure 2). The experimental results for type 0 and type 2 PM are compatible with the expected ones, also in terms of PM resonance frequency; the measured efficiency for type 1 PM is much lower, the reason why is still under analysis.
The PM resonance frequency is strongly dependent on the core Al concentration and geometry, thus offering an effective tunability for this parameter. It is also dependent on the waveguide temperature, which is for this reason actively stabilized during the measurements.

3.2. Pair production

Photon pairs are produced via SPDC by optically pumping at the PM resonance frequency with the NIR laser. The generated photons are split through a 50/50 beam splitter (BS – for type 0 or type 1 PM) or through a polarizing BS (for type 2 PM) and then respectively detected with superconducting nanowire single-photon detectors (*Quantum Opus*). The electrical signals generated by the detectors upon the detection of a photon are fed into a time-to-digital converter (TDC, *quTau*); the coincidence histograms recorded for the three types of phase-matching are shown in Figure 3.
Performances are evaluated in terms of pair production rate (R, net number of measured coincidences per unit integration time, measured in s^{-1}), coincidence-to-accidental ratio (CAR), being the accidental counts the ones collected aside of the signal peak, and brightness (B), defined as R per unit input power and unit bi-photon state bandwidth (measured in $s^{-1}mW^{-1}nm^{-1}$). The obtained results for the different PM types are listed in Table 1: with reference to the state of art peak performances reported in [5], our best results are comparable with the ones of integrated sources with similar characteristics (high compactness and wide bandwidth signal).

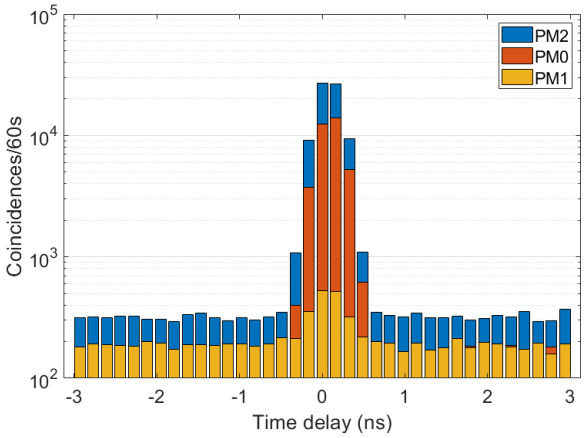

Figure 3: Histograms of coincidences for the three types of conversion processes.

PM	R	B	CAR
0	7.7×10^5	9.6×10^3	34
1	1.2×10^5	1.5×10^3	3.2
2	2.3×10^6	3.8×10^4	78

Table 1: Pair production performances.

3.3. Entanglement visibility

Energy-time entanglement can be demonstrated through a Franson-type interferometry measurement [9]. During this master thesis, we designed and characterized for this scope a fibered Franson interferometer in the folded configuration, which is sketched in Figure 4a. l and s stand for *long* and *short* arm, while ΔL is the length difference between the two. When travelling through the interferometer, each photon (labelled with A or B) will either take l or s after the BS; a coincidence measurement of the OUT signal will reveal three possible combinations of arrival times, according to which path was taken: (i) $s_A - s_B$ and $l_A - l_B$, (ii) $s_A - l_B$ and (iii) $l_A - s_B$. The result is a histogram with a central peak, corresponding to (i), and two satellite peaks for (ii) and (iii), as shown in Figure 4b. Note that the two outcomes in (i) are in principle indistinguishable, hence giving quantum interference. If we post-select the pairs detected in the central peak, their state will be:

$$|\psi_{A,B}\rangle = \frac{1}{\sqrt{2}}\left(|s_A\rangle|s_B\rangle + e^{i2\varphi}|l_A\rangle|l_B\rangle\right). \quad (4)$$

The interfernce pattern is set by the φ value and the visibility of the interference fringes is a figure of merit for the level of entanglement of the generated state: for a separable state it cannot exceed 50%.

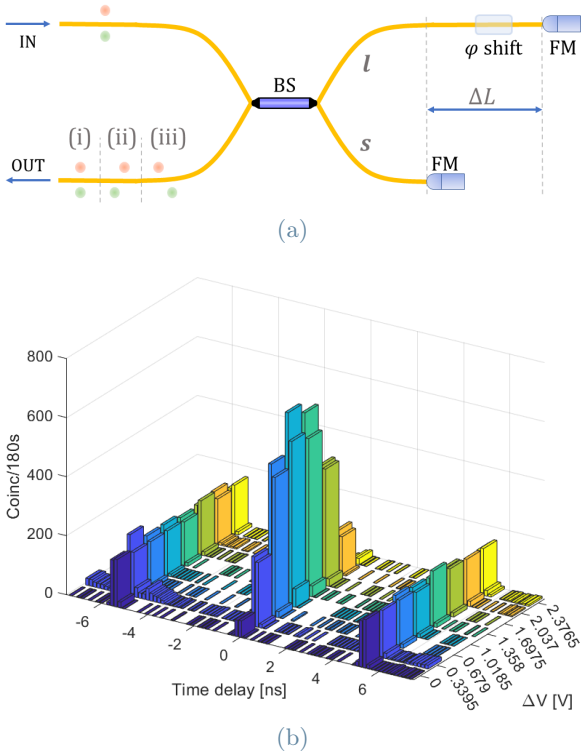

Figure 4: (a) Sketch of the folded Franson interferometer; (b) histogram of coincidences for a Franson measurement.

Some constraints must be respected when designing the interferometer: if ΔT is the is the travelling time difference between the two arms, it must be much larger than the coherence time of each photon, to avoid single-photon interference, and than the combined jitter of detector and TDC, to experimentally distinguish case (i) from (ii) and (iii); moreover, in order to have two-photon interference, ΔT must be much shorter than the pump coherence time.
The phase shift φ is controlled via a piezoelectric fiber stretcher: a different phase value corresponds to each ΔV, as in Figure 4b. Faraday mirrors (FM) are used to compensate for birefringence and for the rotations of polarization experienced within the fiber; a strong thermal isolation or active stabilization is required to avoid thermal phase drifts. Chromatic dispersion, however, is not compensated, introducing a degree of distinguishability between $s_A - s_B$ and $l_A - l_B$, which affects the entanglement visibility: we developed a theoretical model predicting the expected visibility as a function of the signal bandwidth, set by the JSA. The model was experimentally validated, as shown in Figure 5, with the use of a tunable spectral filter, and we were finally able to reach visibilities up to 99%, attesting the high entanglement quality of the state produced with our source.

4. The hybrid AlGaAs/SOI device

Silicon represents one of the leading platforms in linear integrated photonics, thanks to its good mode confinement, moderate optical losses, large-scale high-yield production capability, fabrication maturity (compatible to CMOS processes) enabling the realization of complex integrated optical components. Although nonlinear effects are accessible through its strong third order nonlinear susceptibility, it intrinsically lacks of second order nonlinearity. Furthermore, its indirect bandgap practically prevents it from achieving laser action via electrical pumping. AlGaAs, on the other hand, features both strong $\chi^{(2)}$ and direct bandgap, suitable for electrically injected photon-pair production [10], resulting perfectly complementary to silicon for the implementation of a photonic chip able to generate and manipulate quantum states of light.
We present here a hybrid AlGaAs/SOI device. The AlGaAs stack is bonded on the SOI chip via adhesive bonding, using a layer of benzocyclobutene (BCB) as adhesive and a layer of SiO_2 for relaxing the constraints released once the GaAs substrate is removed from the stack. The AlGaAs waveguides are etched aligned with the silicon ones beneath. Linear tapers are used to

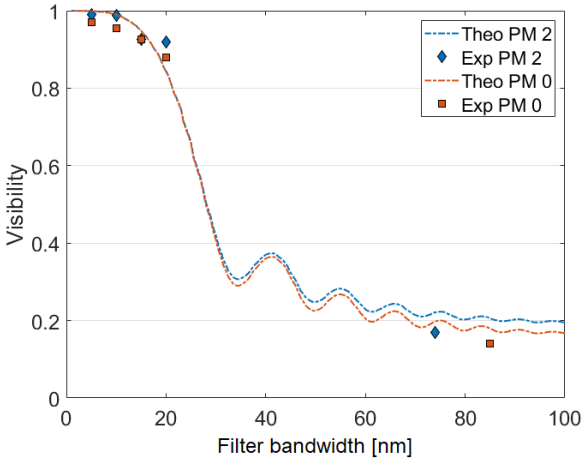

Figure 5: Predicted and experimental Franson visibilities.

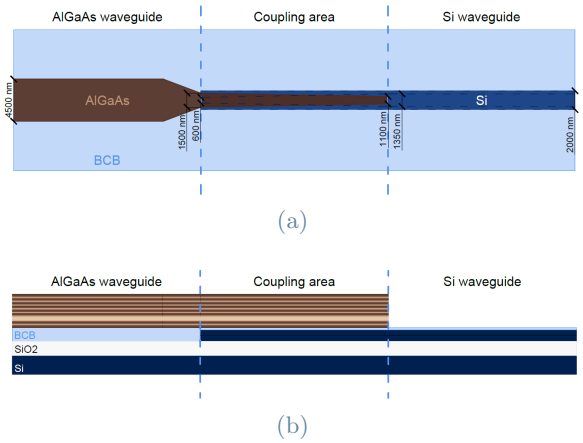

Figure 6: (a) Top and (b) side view of the hybrid device.

achieve evanescent adiabatic coupling between the two waveguides, for the efficient transfer of the optical modes in the telecom range. In Figure 6, the structure design is displayed.
In this first version of the device, photon pairs are expected to be generated via optically pumped SPDC in the AlGaAs waveguide and be transferred to the SOI circuit, where they can be detected and characterized in terms of production performances and entanglement visibility. The initial experimental results demonstrated the mode transmission, validating the efficiency of the designed adiabatic coupling and the successful processing of the taper.

5. Conclusions

In this thesis work, we evaluated the nonlinear efficiency and the pair production performances of monolithic AlGaAs integrated sources, designed for the heterogeneous integration with SOI platforms. The produced quantum state was also characterized in terms of energy-time entanglement visibility, using a fibered Franson interferometer: we demonstrated a visibility up to 99%, confirming the suitability of our sources for QI applications. Finally, we presented a hybrid AlGaAs/SOI device, designed for the on-chip generation and manipulation of quantum states of light.
The next expected steps include the enhancement of type 1 PM conversion processes in our monolithic sources, the realization of a new Franson interferometer featuring chromatic dispersion local compensation, the demonstration of the nonlinear and quantum properties of the hybrid device. On a longer term, we envisage the implementation of an electrically injected hybrid device, with laser action achieved in the AlGaAs waveguide and the produced pairs transferred to the SOI platform for the manipulation and detection.

References

[1] F. Flamini, N. Spagnolo, and F. Sciarrino. Photonic quantum information processing: a review. *Rep. Prog. Phys.*, 82:016001, 2018.

[2] P. Michler. A quantum dot single-photon turnstile device. *Science*, 290:2282–2285, 2000.

[3] Kwiat, P. G. *et al.* New high-intensity source of polarization-entangled photon pairs. *Phys. Rev. Lett.*, 75:4337–4341, 1995.

[4] J. Wang *et al.* Integrated photonic quantum technologies. *Nat. Phot.*, 14:273–284, 2019.

[5] Y. Wang, K. D. Jöns, and Z. Sun. Integrated photon-pair sources with nonlinear optics. *Appl. Phys. Rev.*, 8(011314), 2021.

[6] P. Yeh and A. Yariv. Bragg reflection waveguides. *Opt. Commun.*, 19:427–430, 1976.

[7] A. S. Helmy. Phase matching using Bragg reflection waveguides for monolithic nonlinear optics applications. *Opt. Express*, 14: 1243–1252, 2006.

[8] A. De Rossi *et al.* Measuring propagation loss in a multimode semiconductor waveguide. *J. Appl. Phys.*, 97:073105, 2005.

[9] J. D. Franson. Bell inequality for position and time. *Phys. Rev. Lett.*, 62, 1989.

[10] F. Boitier *et al.* Electrically Injected Photon-Pair Source at Room Temperature. *Phys. Rev. Lett.*, 112:183901, 2014.